PAPER

Vibrational deactivation in $O(^3P) + N_2$ collisions: from an old problem towards its solution

To cite this article: Qizhen Hong *et al* 2022 *Plasma Sources Sci. Technol.* **31** 084008

IOP Publishing Plasma Sources Science and Technology
Plasma Sources Sci. Technol. **31** (2022) 084008 (16pp) https://doi.org/10.1088/1361-6595/ac86f3

Vibrational deactivation in $O(^3P) + N_2$ collisions: from an old problem towards its solution

Qizhen Hong[1,2], Massimiliano Bartolomei[3], Fernando Pirani[4], Fabrizio Esposito[5], Quanhua Sun[1,2] and Cecilia Coletti[6,*]

[1] State Key Laboratory of High Temperature Gas Dynamics, Institute of Mechanics, Chinese Academy of Sciences, 100190 Beijing, People's Republic of China
[2] School of Engineering Science, University of Chinese Academy of Sciences, Beijing 100049, People's Republic of China
[3] Instituto de Física Fundamental—CSIC, C/ Serrano 123, Madrid, Spain
[4] Dipartimento di Chimica, Biologia e Biotecnologie, Università di Perugia, via Elce di Sotto 8, 06183 Perugia, Italy
[5] Consiglio Nazionale delle Ricerche, Istituto per la Scienza e Tecnologia dei Plasmi, Sede Secondaria di Bari, via Amendola 122/D 70126 Bari, Italy
[6] Dipartimento di Farmacia, Università G. d'Annunzio Chieti-Pescara, via dei Vestini, 66100 Chieti, Italy

E-mail: ccoletti@unich.it

Received 1 June 2022, revised 19 July 2022
Accepted for publication 4 August 2022
Published 30 August 2022

Abstract

In a recent communication [2021 *Phys. Chem. Chem. Phys.* **23** 15475–79] we showed that the correct modelling of vibrational quenching events in $O + N_2(v)$ collisions, a fundamental process in air plasmas, requires the detailed representation of intermediate and asymptotic regions of the interaction and the inclusion of several types of processes as vibration to translation (V–T) and vibro-electronic (V–E) energy transfer. For the first time from the publication of experimental results in the 70's, we obtained theoretical results in agreement with experiments, even at room temperature. In the present work we extend the approach to better describe non-adiabatic V–E deactivation and include the evaluation of the role of the higher excited singlet N_2O surface, characterized by new high quality *ab initio* calculations, to that of the triplet Π and Σ ones. Within this framework, we calculate V–T, V–E and the corresponding total vibrational relaxation rate coefficients for initial vibrational $N_2(v)$ quantum numbers up to $v = 10$ in a wide temperature range (200–10 000 K). These data are of uttermost importance for the modelling of air plasmas, of earth's and planetary atmospheres and for the design and construction of aircrafts and air-breathing propulsion systems for very low earth orbit (VLEO) satellites.

Keywords: vibrational relaxation, non-adiabatic transitions, $N_2 + O$ collisions, V–T rate coefficients, V–E rate coefficients

Supplementary material for this article is available online

(Some figures may appear in colour only in the online journal)

* Author to whom any correspondence should be addressed.

1. Introduction

Non-thermal air plasmas are characterized by strong non-equilibrium conditions, in particular relative to molecular vibration, which make their modelling a non trivial task [1–3]. As a consequence, the adoption of detailed state-to-state models, including a wealth of reactive, inelastic and dissociation rate coefficients relative to electron–molecule, molecule–molecule and molecule–surface collisions, is needed [4].

On the other hand, technological applications of air plasma are wide and continuously expanding, ranging from electrical discharges [5], combustion chemistry [6], aircraft re-entry processes in a hypersonic flight regime [7, 8] at high temperature. The importance of cold plasmas is also rapidly rising in medical applications [9] and for nitrogen fixation [10], whereby nitrogen molecules are converted in reactive nitrogen, a promising alternative to the currently used Bosch–Haber process. Moreover, low temperature planetary atmospheres (including earth) are often found in non-local thermal equilibrium conditions and their modelling also requires the knowledge of accurate and detailed vibrational state-to-state data for specific collision processes involving air species [11].

The vast majority of such data can seldom be obtained from experiments and, even when they are available, they are limited to low vibrational quantum numbers of the involved molecular species (ground and first excited vibrational levels in most cases). The rate coefficients needed to cover a sufficiently large number of states for the complete kinetic modelling are often extrapolated by relying on simple models with very rough approximation and low level of detail. Because the efficiency of most of the above mentioned applications strictly depends on the plasma operating conditions, the reliability of its modelling is a crucial issue, and so is the reliability of the rate coefficients used for such models.

In the last years, we calculated vibration-to-vibration (V–V) and vibration-to-translation (V–T) rate coefficients databases for a wide range of temperature and vibrational quantum numbers in diatom–diatom collisions [12–14]. We used a mixed-quantum classical dynamics approach (so to recover the most relevant quantum effects in the investigated systems) and potential energy surfaces (PESs) able to correctly describe the long range interaction region (as well as the interaction wells and first repulsive walls), important for the accurate reproduction of inelastic collisions. More recently [15], we started investigating vibrational relaxation in $N_2 + O$ inelastic collisions, a very intriguing system because of the many possible (inelastic, reactive, non-adiabatic) channels available upon collision. In addition, molecular nitrogen and atomic oxygen are the reactive species in the first Zeldovich reaction ($O + N_2(v) \rightarrow NO(v') + N$), crucial for nitrogen fixation in cold plasmas [16], whose fate is also determined by the availability of vibrationally excited nitrogen.

The exchange of vibrational energy quanta in inelastic collisions with atomic oxygen is in fact one of the main processes determining the molecular nitrogen vibrational population in the non equilibrium conditions characterizing air plasmas and has therefore long been studied, both experimentally [17–19] and theoretically [20–23].

However, calculated and experimental rate coefficients failed to match, showing differences of some factors (in the best case) at high temperature and up to orders of magnitude in the 300–1000 K range, critical for applications in low temperature air plasmas or for air-breathing propulsion systems, as those used in the development of very low earth orbit (VLEO) satellites [24].

The solution to this problem was found in reference [15], where we showed that vibration-to-translation (V–T) collisional events are not the only responsible for nitrogen vibrational quenching, since vibration-to-electronic (V–E) energy transfer processes, triggered by the electronic anisotropy of the open shell $O(^3P_J)$ atom, are very effective, and in fact dominating, at low temperature. Moreover, the quantitative assessment of the $O(^3P_J)$ behavior also depends on the atomic spin–orbit coupling, which leads to fine levels identified by the total electronic quantum number $J = 2, 1, 0$. The importance of non-adiabatic transitions between different spin–orbit PESs when atomic oxygen is involved in the collisional dynamics had been hinted by Nikitin and Umanski [25] as early as 1972. Subsequently, adiabatic potential energy curves and non adiabatic coupling terms between them have been properly characterized by analyzing molecular beam experiments concerning the scattering of $O(^3P_J)$ atoms, analyzed in state and selected in their magnetic sublevels, by noble gas targets [26]. The neglect of V–E energy transfer processes is indeed the main reason for the failure of calculated rate coefficients to reproduce experimental data: by including their contribution, evaluated by a simple Landau–Zener approach (considering only collinear collisions), we were able to obtain total vibrational relaxation coefficients in very good agreement with measured values.

Here we extend our previous work to calculate all the contributions to the vibrational quenching of $N_2(v)$ by $O(^3P)$ collisions for vibrational quantum numbers v up to 10. Due to the complex manifold of the electronic and spin orbit states of the system, loss of vibrational energy can occur, as mentioned above, either by V–T or by V–E energy transfer. We use a mixed quantum–classical (MQC) method for the V–T rate coefficients calculation, having previously experimented the limited accuracy of quasiclassical trajectory method at low collision energy in treating vibrationally inelastic processes for the present collisional system [15, 20]. For the calculation of V–E rate coefficients, similarly to our previous work in [15], we use Landau–Zener approaches, but in the present case we include configurations different from the collinear one and take into account surface crossings with the singlet state of the system. It is worth noting that this non-adiabatic path through the N_2O singlet has been the first proposed in the literature for explaining the discrepancies with experiments [27], but it has been noted that the threshold for this process is too high to explain any contributions at room temperature.

In details, in section 2 we describe the spin–orbit and electronic states which can contribute to the vibrational quenching of the system together with the available PESs.

Potential energy curves for specific geometries of the electronically excited singlet state (involving $O(^1D)$ state) have been obtained by new *ab initio* calculations. Section 3 reports on the rate coefficients calculation for the V–T and V–E processes, providing values for the $N_2(v = 1) + O \rightarrow N_2(v = 0) + O$ quenching (the only process for which experimental data are available), for the $N_2(v) + O \rightarrow N_2(v - 1) + O$ process, involving the loss of one vibrational energy quantum, for which we also give a general analytical expression for rate coefficients as a function of temperature, and for the $N_2(v) + O \rightarrow N_2(v - \Delta v) + O$ multiquantum relaxation. The contribution of each deactivation process to the overall vibrational quenching is analyzed and discussed. A final section, highlighting future perspectives to overcome limitations/approximations of some of the employed methodologies, concludes the paper.

2. Phenomenology of spin–orbit and electronic states and their PESs

One of the challenges in the modelling of the dynamics of $O(^3P) + N_2(X^1\Sigma)$ collisions is the description of the complex manifold of the involved spin–orbit and electronic states, mostly arising because of the open shell nature of oxygen atom.

The lowest PESs represent the interaction in the two triplet states of Π symmetry (i.e. with electronic molecular quantum number $\Lambda = 1$). They are obtained when the oxygen atom approaches the $N_2(X^1\Sigma)$ molecule with one of the half filled p orbitals pointing towards the molecular center of mass in the collinear $C_{\infty v}$ configuration. In a more general picture, this configuration correlates with two different orientations of the fully occupied p orbital of oxygen $O(^3P)$ (figure 1), leading to the $1^3A''$ and $1^3A'$ states in C_s symmetry. These states are close in energy and are degenerate in the $C_{\infty v}$ geometry, and correlate with $^3B_2$ and $^3B_1$ symmetries, respectively, in a perpendicular C_{2v} configuration. These states of Π character tend to become asymptotically degenerate since they correlate with the oxygen atom in its ground $^3P_2$ fine level. The same states are expected to be substantially different only in the strongly interacting region, where the overlap of external orbitals opens the reaction channels leading to $N(^4S) + NO(^2\Pi)$.

When the oxygen atom approaches the nitrogen molecule in the $C_{\infty v}$ configuration, pointing with the only filled p orbital towards the molecular center of mass, a single $^3\Sigma$ state is obtained (electronic molecular quantum number $\Lambda = 0$), which transforms in $2^3A''$ and $^3A_2$ in C_s and C_{2v} symmetry, respectively. The state of Σ character asymptotically correlates with the excited spin–orbit level $O(^3P_0)$ that lies 28.1 meV in energy above $O(^3P_2)$. Moreover, at short distance the Σ state correlates with the reactive channel $N(^2D) + NO(X^2\Pi)$, which is 5.7 eV higher in energy, and not easily accessible. Because of this, $O(^3P_0) + N_2(X^1\Sigma)$ collisions are most often considered as non reactive.

Detailed considerations on the fine structure of open shell species indicate that O atoms in their ground ^3P electronic state also involve, in addition to $^3P_2$ and $^3P_0$, the $^3P_1$ fine level, that is located about 20 meV above the lowest $^3P_2$ state. It has been demonstrated [26] that the interaction of $O(^3P_1)$ with a closed shell partner forms adducts having 1/3 and 2/3 of Π and Σ character, respectively. Therefore, taking into account, as stressed above, that $O(^3P_2)$ and $O(^3P_0)$ form adducts with pure Π and Σ character, respectively, the present analysis has been performed assuming that $O(^3P_{2,1,0})$ atoms globally interact with 2/3 and 1/3 of Π and Σ character. This assumption is valid if the three fine levels are statistically populated (approximately in the 5:3:1 ratio), a condition that is fulfilled for bulk (plasmas) temperatures higher than 500 K. At lower temperature the population of Π character states becomes progressively higher.

States involving electronically excited oxygen atoms are higher in energy. The lowest singlet state $1^1A'$ ($^1\Sigma$) correlates with $O(^1D) + N_2(X^1\Sigma)$ and asymptotically lies 1.97 eV above the $^3\Pi$ states [28]. The PESs involving $O(^1S)$, or electronically excited N_2 to its $^1\Sigma_u^+$, $^3\Pi_g$, or $^3\Delta_u$ states, are even higher in energy and cannot be populated nor contribute in any way at the temperature range considered in the present work.

In the last years, depending on the studied processes, a number of PESs have been formulated for the various states. PESs for the $1^3A''$ and $1^3A'$ states allow to investigate the forward $N + NO \rightarrow N_2 + O$ and inverse $N_2 + O \rightarrow N + NO$ reactions and have been obtained, among others, by Gamallo *et al* [29], by Lin *et al* [30] (specifically designed for high energy collisions) and by Meuwly and coworkers [21, 22]. They are based on the fitting of high level (MRCI or CASPT2) *ab initio* points of triple zeta quality. Calculated QCT rate coefficients [20, 22, 30–32] for the direct and inverse reactions based on these surface pairs are in good agreement with the experimental values. However, large discrepancies with measured data are found when they are used for the calculation of vibrational relaxation rates for $N_2(v = 1) + O(^3P)$ collisions, particularly at low temperature. As we discussed in [15], this behavior might be related to a less accurate description of the long range interaction region, which can be crucial for the outcome of energy transfer processes. Indeed, orientation and alignment effects start at long range and determine the formation of precursor configurations strongly affecting the collision dynamics. Because of the very large number of points needed to cover the long range region, *ab initio* based potentials often make use of fitting procedures on a limited number of weakly interacting configurations, which may lead to inaccuracies at the longest interaction distances. This is basically the reason why in reference [30] the authors specifically recommend the use of their PESs for the endothermic reaction at high collision energy. The PESs of references [22, 29], which instead have also been used at low collision energy as well as for inelastic scattering, were found to present some inaccuracies at long range, like a non-degenerate behavior of the two $^3\Pi$ PESs for the collinear configuration (figure S1 (https://stacks.iop.org/PSST/31/084008/mmedia)). This is more marked for the potential in reference [22] where the $1^3A''$ and $1^3A'$ diverge for interaction distances $R \geqslant 4.5$ Å where they present early barriers and a well. Note that such discrepancy at long range has negligible consequences on the description of the reaction dynamics, dominated by short range interactions, but

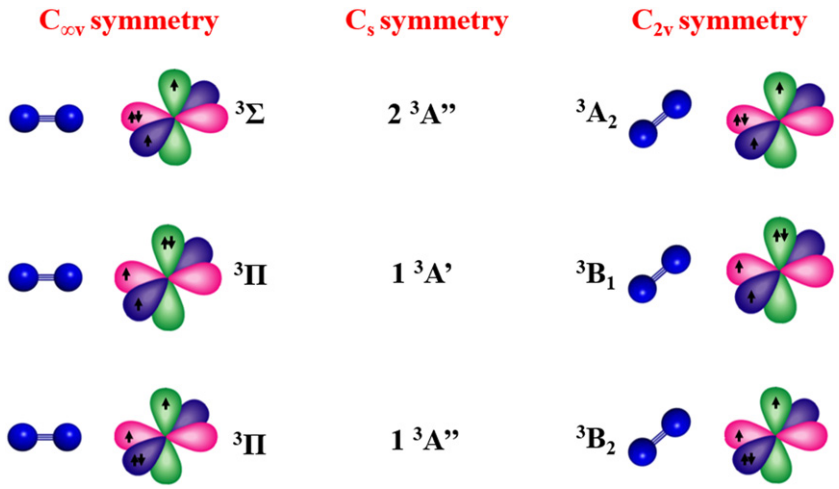

Figure 1. Correlations of the considered PESs under different symmetries of the $O(^3P) + N_2$ complex.

becomes crucial in the description of low temperature inelastic collisions.

To correctly represent the long and medium range behavior for $O(^3P) + N_2(X^1\Sigma)$ collisions and accurately calculate the vibrational relaxation rates, we recently introduced an analytic non-reactive PES [15] describing the $^3\Pi$ potential (considered as an average contribution of the $1^3A''$ and $1^3A'$ states) based on the Improved Lennard Jones model [33]. Such PES, containing physically meaningful parameters, modulated and benchmarked against scattering experiments performed in the thermal collision energy range and *ab initio* points, gives excellent results in the comparison between calculated and experimental rate coefficients for the vibrational quenching in $N_2(v = 1) + O(^3P)$ collisions (see next section).

In the same work we also introduced a PES for the $^3\Sigma$ ($2^3A''$) state, which is much less studied than the $^3\Pi$, $1^3A''$ and $1^3A'$, states, because of its mainly non-reactive character (as mentioned above, the reactive channel opens at very high energies). As a matter of fact, to the best of our knowledge the only previous formulation was performed by Nakamura and Kato [34] who built PESs for all the triplet states $1^3A''$, $1^3A'$ ($^3\Pi$) and $2^3A''$ ($^3\Sigma$) based on 520 CASSCF *ab initio* points and the singlet $1^1A'$ ($^1\Sigma$) state, based on 1160 points to evaluate the decay from singlet to triplet states and the non-adiabatic spin-forbidden predissociation $N_2O(X^1\Sigma^+) \rightarrow O(^3P) + N_2(X^1\Sigma)$. Although the $^3\Sigma$ potential has received much less attention than the two $^3\Pi$ PESs, it is worth pointing out again that 1/3 of $O(^3P) + N_2(X^1\Sigma)$ collisions begin from this state and that it is determinant for the description of non-adiabatic vibro-electronic relaxation [15], as shown in the following.

The N_2O singlet PES, $1^1A'$, correlating with the $O(^1D) + N_2(X^1\Sigma)$ was described, among others, by Nakamura and Kato [34], Gonzaléz *et al* [35] and by Li and Varandas [36]. It has been argued [27] that, though lying higher in energy than the triplet PESs, it could contribute to the vibrational quenching of $O(^3P) + N_2(X^1\Sigma)$ at high collision energies, when a crossing might occur involving the vibrationally excited N_2 molecule. To properly investigate that crossing, we have therefore obtained the potential energy curves corresponding to the parallel and perpendicular approach geometries for the ground singlet state, which asymptotically correlates with the $O(^1D) + N_2(X\ ^1\Sigma_g^+)$ fragments. To do that we rely on a multiconfigurational ansatz and here we apply an approach already exploited to obtain interaction energies for spin multiplicity states lower than the maximum one of the $(O_2)_2$ [37, 38] and $(O_2)_4$ [39] complexes. In this approach we treat the highest spin (triplet) complex by means of a restricted coupled cluster theory with single, double, and perturbative triple excitations [RCCSD(T)]. In addition, the singlet-triplet splitting can be well described at the multiconfigurational complete active space self-consistent field (CASSCF) theory, provided that a sufficiently extended active space is taken into account. Finally, our best estimate of the N_2O singlet energies is obtained by adding to the RCCSD(T) triplet potential the singlet-triplet CASSCF splitting. The RCCSD(T) triplet interaction energies are those previously obtained in reference [15] and they refer to a complete basis set extrapolation while CASSCF energies have been here obtained by using the aug-cc-pVQZ basis set. For the CASSCF calculations, the active space is defined by distributing sixteen electrons in sixteen molecular orbitals correlating asymptotically with the N_2 $(2, 3)\sigma_g(2, 3)\sigma_u 1\pi_u 1\pi_u$ and O (2, 3)s(2, 3)p shells. All calculations have been performed by employing the Molpro code [40] and by fixing the N_2 distance to 1.1007 Å, its equilibrium value.

In this work we calculated V–T and V–E rate coefficients to obtain total vibrational relaxation rates for $O(^3P) + N_2(X^1\Sigma)$ collisions by using the triplet Π and Σ PESs we introduced in reference [15] and the potential energy curves for the parallel and perpendicular configurations of the singlet Σ state obtained herein. The curves corresponding to the parallel and perpendicular configurations for these PESs, together with the calculated *ab initio* points are summarized in figure 2. We note here that the agreement between the analytical PESs and the *ab initio* points is excellent at long range, in the well and in the first repulsive region, whereas the repulsive

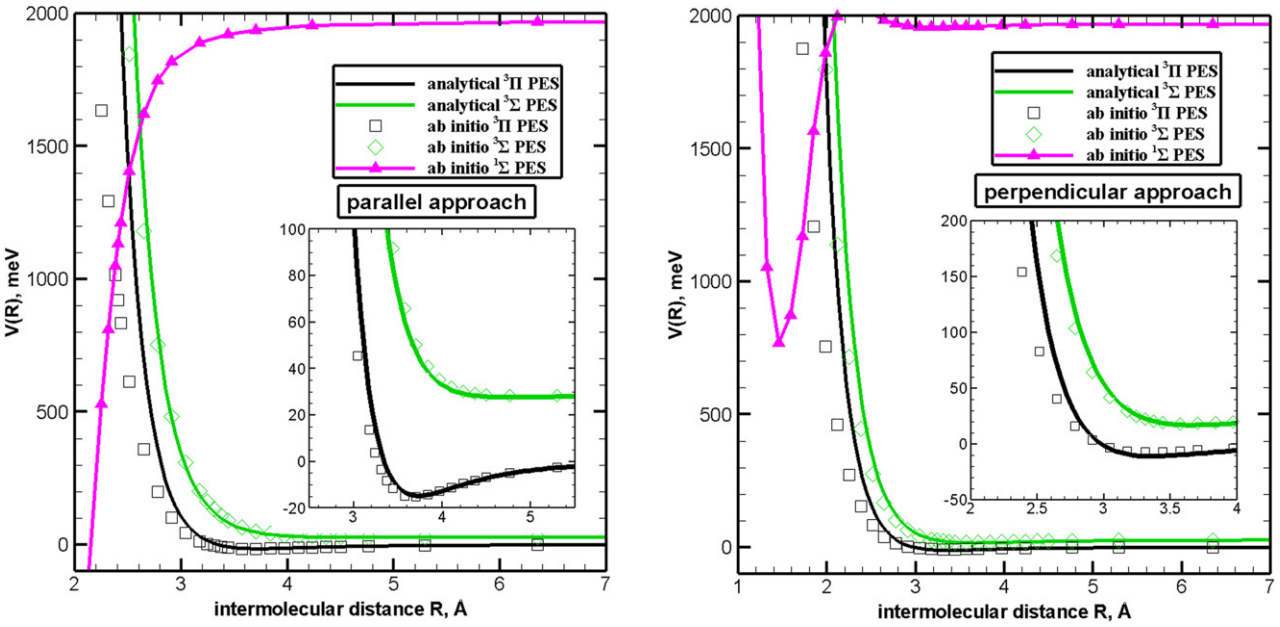

Figure 2. Behavior of different PESs as a function of the intermolecular distance R for the parallel (left panel) and perpendicular (right panel) configurations.

wall in the strong interacting region is clearly anticipated by the analytical curves, particularly for the $^3\Pi$ reactive surface. This is expected in the case of non-reactive potentials. The implications of such behavior will be thoroughly discussed in the following sections.

3. Vibrational relaxation rates

The quenching of vibrationally excited nitrogen molecules $N_2(X^1\Sigma_g^+)$ by oxygen atom $O(^3P)$ collisions can occur either by vibration to translation (V–T) or vibration to electronic (V–E) energy transfer. We recently showed [15] that a very good agreement between calculated and experimental rate coefficients for the relaxation of $N_2(v = 1)$ is obtained in the temperature range 300–4500 K with V–T rates (dominating at high temperature) calculated by a MQC method [41] and V–E rates (dominating at low temperature) computed by a simple Landau–Zener approach [42–44], where only the prevailing contribution of collinear collisions was considered. In the following we will use the same MQC method to describe V–T processes and will extend the Landau–Zener approach to include, on one hand, perpendicular collisions and, on the other, to treat crossings between the triplet and singlet PESs, which were neglected in our previous work. Furthermore, we will consider vibrational relaxation of excited N_2 up to $v = 10$ in the temperature range 300–10 000 K. Above 5000 K reactivity, also stimulated by vibrational excitation, becomes increasingly important. Nonetheless the present non-reactive PES is still expected to describe well the relaxation dynamics of the system: inelastic rate coefficients calculated by using the same method on the present and on the reactive PES of reference [29] show differences of a factor 2.5 at most [15] at $T \geqslant$ 5000 K.

3.1. V–T rate coefficients calculation: the mixed quantum–classical method

The MQC method (often referred to as semiclassical) can be effectively used for the description of V–T (and V–V, vibration to vibration energy transfer [12, 13, 45]) processes, as it allows to recover most quantum effects associated to the vibrational motion (quantum tunnelling, zero point energy, etc) in a classical framework, thus taking advantage of the computational efficiency of quasi-classical calculations, particularly important when considering heavy particles. The present approach describes the N_2 vibration and the associated rotovibrational coupling by quantum mechanics, using a Morse wavefunction (whose parameters are given in table S1) and solves the corresponding time-dependent Schrödinger equation through a close coupled equations method. Translation and rotational motions are treated by classical mechanics, solving Hamilton equations of motion. The coupling of the two subsystems is obtained through the use of an Ehrenfest averaged potential, defined as the quantum expectation value of the interaction potential. This method provides accurate quantum transition probabilities and properly conserves total (quantum plus classical) energy. Details on the method can be found in reference [41] and in supporting information. In the present work, V–T rate coefficients were obtained by considering 47 initial values of total classical (translation + rotation) energy comprised between 50 and 80 000 cm^{-1}, with a more frequent sampling directed towards lower energies. For each energy value, 5000 trajectories were used, as well as an initial separation distance atom-diatom R equals to 50 Å and an impact parameter randomly chosen between 0 and 9 Å. The set of coupled time-dependent quantum equations to be solved for the vibrational motion comprises vibrational states v that satisfy $\Delta v = \pm 8$. These

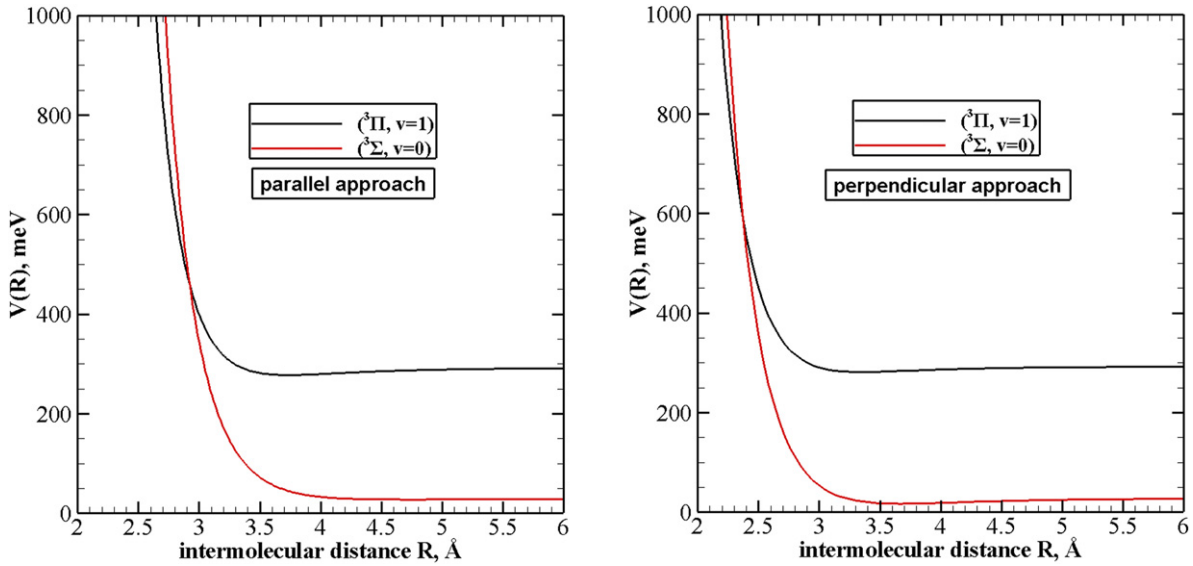

Figure 3. Potential curves for the $N_2(X^1\Sigma_g^+) + O(^3P)$ interaction with N_2 molecular axis oriented parallel (left panel) and perpendicular (right panel) to the intermolecular distance. The N_2 molecule is assumed in the first excited $v = 1$ vibrational level for the $^3\Pi$ state, while for the $^3\Sigma$ state $v = 0$ is considered.

parameters should give a V–T data uncertainty between 10 and 20%.

3.2. Vibrational relaxation for $N_2(v = 1) + O \rightarrow N_2(v = 0) + O$

Vibrational relaxation of $N_2(v = 1)$ upon collision with oxygen atoms has been extensively investigated by experiments [17–19] in the 300–4500 K temperature range as well as theoretically [20, 22, 32] by calculating V–T rates. The latter studies, however, nearly invariably underestimate the measured values (with the exception of reference [22] where rate coefficients were underestimated in the low and overestimated in the high temperature regimes), with huge differences at temperature $\leqslant$1000 K. As mentioned before, we recently demonstrated [15] that this discrepancy is caused by the neglecting of V–E energy transfer which indeed turns out to be crucial for vibrational quenching when oxygen atoms are involved [25].

In particular, the crossings between the vibronic $^3\Pi$ and $^3\Sigma$ surfaces occur at energy values small enough for the corresponding energy transfer process (hereafter indicated as V-E1) to be effective at low temperature. Such crossing in the parallel $C_{\infty v}$ configuration can be located, by using the PESs of reference [15], at $R_c = 2.922$ Å and at an energy value $E_c = 0.4592$ eV (figure 3 and table 1). Collisions in the $C_{\infty v}$ symmetry are expected to be the most effective for V–E energy transfer and therefore were the only contribution considered in [15]. Here we also evaluate the contribution coming from collisions in the C_{2v}, perpendicular, symmetry for which the crossing point occurs at $R_c = 2.373$ Å and the potential energy is $E_c = 0.5915$ eV.

The V–E rate coefficients are given by

$$k_{V-E}(T) = \sqrt{\frac{8k_BT}{\pi\mu}}\frac{1}{(k_BT)^2}\int_0^\infty \sigma(E)e^{-E/k_BT}EdE, \qquad (1)$$

where μ is the reduced mass, E is the collision energy (here taken from 0 to 10 eV), k_B is the Boltzmann constant and the cross sections $\sigma(E)$ are calculated as

$$\sigma(E) = \frac{\pi}{k^2}\sum_{l=0}^{l_{max}}(2l+1)\cdot P \qquad (2)$$

with

$$P = 2P_x(1-P_x), \qquad (3)$$

in which P_x is the probability of the system to remain on the same surface, $(1 - P_x)$ is that of changing surface, and $k^2 = \frac{2\mu E}{\hbar^2}$. For the $\left(^3\Pi, v = 1\right) \rightarrow \left(^3\Sigma, v = 0\right)$ crossing $P_x = P_{1,0}$ in table 1.

The V-E1 P_x probability is obtained here applying the original Landau–Zener method [42–44] to the collinear and perpendicular configurations according to:

$$P_x = \exp\left(-\frac{2\pi H^2}{\hbar v_R \Delta}\right), \qquad (4)$$

where v_R is the radial velocity at the crossing, Δ is the difference between the slope of the two PESs at the crossing point (table 1) and H is the coupling between the two PESs. Details on the evaluation of v_R and of the H coupling term are given in the appendix A. Because of the approximations involved in the method and in the estimate of H, the obtained V-E1 rate coefficients are expected to be less accurate (about 50% estimated uncertainty) than V–T rates for the homologous processes. Note that the Franck–Condon factor is taken equal to 1, as expected on the basis of the involved vibrational levels.

Figure 4 reports $(^3\Pi, v = 1) \rightarrow (^3\Sigma, v = 0)$ V-E1 rate coefficients for the parallel and perpendicular configurations multiplied by 1/3 and 2/3, respectively, i.e. their contributions to the total V-E1 rates. V-E1 rates were further multiplied by 2/3, the fraction of $^3\Pi$ state population. Calculated rates

Table 1. Crossing points in parallel and perpendicular configurations for non adiabatic transitions with $\Delta v = 1$: R_c is the position, E_c is the potential energy and Δ is the absolute difference of the curve slopes.

		Parallel			Perpendicular		
Crossing point between	P_x	R_c (Å)	E_c (eV)	Δ (eV Å^{-1})	R_c (Å)	E_c (eV)	Δ (eV Å^{-1})
$\left({}^3\prod, v=1\right)$ and $\left({}^3\sum, v=0\right)$	$P_{1,0}$	2.922	0.459	0.785	2.373	0.592	0.878
$\left({}^3\prod, v=2\right)$ and $\left({}^3\sum, v=1\right)$	$P_{2,1}$	2.930	0.739	0.785	2.380	0.867	0.878
$\left({}^3\prod, v=3\right)$ and $\left({}^3\sum, v=2\right)$	$P_{3,2}$	2.937	1.015	0.785	2.385	1.143	0.878
$\left({}^3\prod, v=4\right)$ and $\left({}^3\sum, v=3\right)$	$P_{4,3}$	2.940	1.290	0.737	2.388	1.417	0.878
$\left({}^3\prod, v=5\right)$ and $\left({}^3\sum, v=4\right)$	$P_{5,4}$	2.945	1.561	0.737	2.392	1.686	0.840
$\left({}^3\prod, v=6\right)$ and $\left({}^3\sum, v=5\right)$	$P_{6,5}$	2.950	1.828	0.705	2.397	1.951	0.840
$\left({}^3\prod, v=7\right)$ and $\left({}^3\sum, v=6\right)$	$P_{7,6}$	2.955	2.091	0.705	2.401	2.214	0.840
$\left({}^3\prod, v=8\right)$ and $\left({}^3\sum, v=7\right)$	$P_{8,7}$	2.960	2.351	0.705	2.405	2.472	0.802
$\left({}^3\prod, v=9\right)$ and $\left({}^3\sum, v=8\right)$	$P_{9,8}$	2.965	2.608	0.675	2.410	2.727	0.802
$\left({}^3\prod, v=10\right)$ and $\left({}^3\sum, v=9\right)$	$P_{10,9}$	2.971	2.861	0.675	2.414	2.979	0.802

for both configurations at different temperature values can be found in tables S2 in the supporting information.

V-E1 rate coefficients for collisions occurring in the perpendicular configuration (the blue dashed line) are very small at temperature lower than 700–800 K, but their contribution increases with temperature and becomes equal to that calculated for the parallel configuration at $T = 4000$ K. The results show that rate coefficients calculated for the perpendicular geometry in practice cannot be neglected for temperature higher than 1000 K.

In the present work we extended the Landau–Zener approach to include the evaluation of the excited singlet N_2O surface role in the description of non-adiabatic V–E deactivation. The non-adiabatic transition from the triplet to singlet surface (hereafter indicated as V-E2) was indeed suggested to be a possible mechanism contributing to the overall vibrational quenching at temperature higher than 600 K [27]. Therefore, we explicitly calculated probabilities and rate coefficients for the vibrational deactivation events of $N_2(X^1\Sigma_g^+, v = 1) + O(^3P)$, which first jumps to singlet PES ($v = 0$) through the non-adiabatic transition and then goes back to the triplet PES vibrational ground state $N_2(X^1\Sigma_g^+, v = 0) + O(^3P)$.

The crossing points between the singlet PES and the triplet ones were characterized by *ab initio* points consistently calculated, as described in section 2. The *ab initio* potential energy curves in the parallel and perpendicular configurations are displayed as a function of the intermolecular distance R (with the N_2 distance fixed at its equilibrium value) in the left and right panels of figure 5, respectively. In the figure, the *ab initio* singlet PES is shown along with the *ab initio* data of vibronic $^3\Pi$ and $^3\Sigma$ PESs for $N_2(v = 0)$ and $N_2(v = 1)$. The details of the crossing points are given in table 2, which shows that the singlet curve crosses the *ab initio* vibronic states ($^3\Pi$, $v = 0$) and ($^3\Pi$, $v = 1$) at $R = 2.377$ Å and 2.420 Å respectively, for the parallel and at $R = 1.807$ Å and 1.844 Å for the perpendicular configuration. The energy barrier for the V-E2 non adiabatic crossing is 0.878 eV in the parallel configuration, which is close to the 0.8 eV value reported by Fisher and Bauer [27]. For the perpendicular configuration a larger barrier is found due to the decreased well depth of the N_2O singlet surface.

Specifically, three V-E2 independent cases can be considered (table 2): starting from the vibrationally excited $^3\Pi$ PES ($^3\Pi$, $v = 1$) surface and ending on the same vibrational ground state PES ($^3\Pi$, $v = 0$) (case 1); starting from the vibrationally excited $^3\Sigma$ PES ($^3\Sigma$, $v = 1$) surface to end on the vibrational ground state $^3\Pi$ PES (case 2) or $^3\Sigma$ PES (case 3).

For the calculation of V-E2 energy transfer probability a different treatment than the original Landau–Zener method is required, because the two crossing curves have now effective opposite sign slopes (figure 5). In such cases, a modified Landau–Zener method has been developed [46, 47], which considers the role of metastable bound states. According to an extended quantum formulation first suggested by Landau [46, 47] the transition probability can now be calculated as:

$$P_x = 1 - \beta^{4/3}\pi^2 Ai^2\left(-\beta^{2/3}\varepsilon\right), \tag{5}$$

where P_x is the probability of the system staying on the same surface, $\mathrm{Ai}(x)$ is the Airy function and β and ε depend on the slope of the crossing curves and on the coupling term H, as detailed in the appendix A.

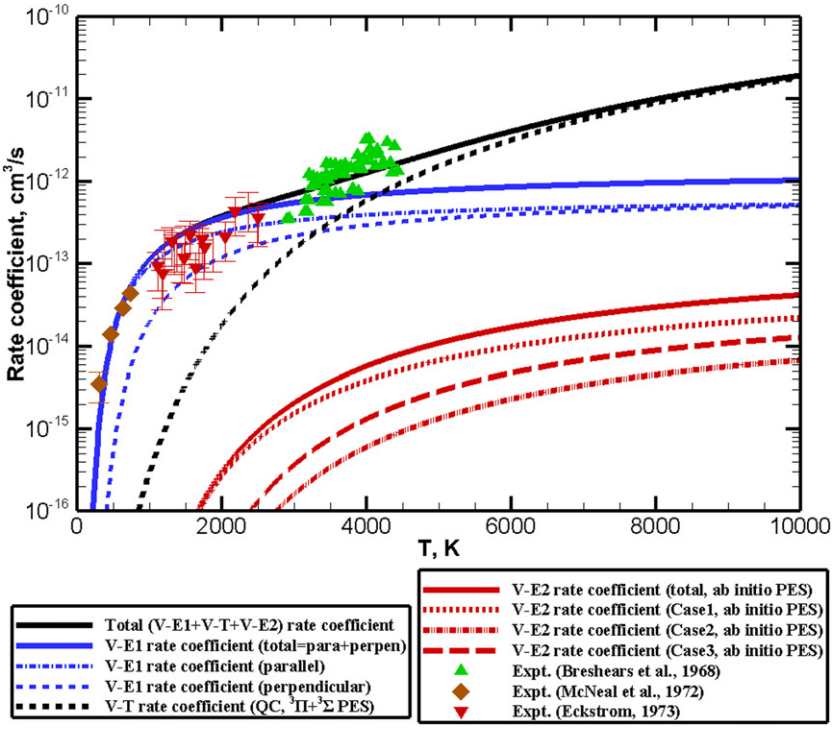

Figure 4. Rate coefficients for vibrational relaxation upon $N_2(X^1\Sigma_g^+)(v = 1) + O(^3P)$ collision as a function of temperature. Experimental data obtained by Eckstrom [18] in the 1200–3000 K range by shock-tube experiments, by Breshears and Bird [17] in the 3000–4500 K range, also by shock-tube experiments, and, at lower temperatures (300–740 K), by McNeal *et al* [19] through photo-ionization, are also reported.

Table 2. Crossing points in parallel and perpendicular configurations. R_c is the position and E_c is the potential energy.

	Parallel		Perpendicular	
Crossing point between	R_c (Å)	E_c (eV)	R_c (Å)	E_c (eV)
$(^3\Pi, v = 1) \rightarrow (^1\Sigma, v = 0) \rightarrow (^3\Pi, v = 0)$	2.420	1.171	1.844	1.542
Case 1	2.377	1.034	1.807	1.433
$(^3\Sigma, v = 1) \rightarrow (^1\Sigma, v = 0) \rightarrow (^3\Pi, v = 0)$	2.624	1.586	2.022	1.900
Case 2	2.377	1.034	1.807	1.433
$(^3\Sigma, v = 1) \rightarrow (^1\Sigma, v = 0) \rightarrow (^3\Sigma, v = 0)$	2.624	1.586	2.022	1.900
Case 3	2.580	1.514	1.978	1.846

The total probability for the non-adiabatic transition event $(^3\Pi, v = 1) \rightarrow (^1\Sigma, v = 0) \rightarrow (^3\Pi, v = 0)$ process (case 1) is:

$$P = 2P_2(1 - P_2) \cdot (1 - P_1), \tag{6}$$

where $1 - P_1$ and $1 - P_2$ are the transition probabilities of $(^3\Pi, v = 1) \rightarrow (^1\Sigma, v = 0)$ and $(^1\Sigma, v = 0) \rightarrow (^3\Pi, v = 0)$, respectively. The V-E2 probabilities of cases 2 and 3 can be obtained in the similar way.

From these values the corresponding cross sections and rate coefficients are calculated by equations (1) and (2), respectively. The same considerations made on the uncertainty of calculated V-E1 rate coefficients hold for V-E2 ones: an uncertainty of 50% ca. is expected. In addition, the Franck–Condon factor is assumed to be one, which means that the present results should provide an upper limit to the correct rate coefficients.

Figure 4 shows (as red lines) rate coefficients for all V-E2 processes with the orientation weight and $^3\Pi$ and $^3\Sigma$ proportions already taken into account. Calculated data at selected temperature values can be found in tables S3 in the supporting information. In order to double check our results, we also calculated V-E2 rate coefficients for case 1 by using the $^3\Pi$ and $^1\Sigma$ PESs given in reference [34] by Kato and Nakamura (figure S2 in supporting information), which, though slightly smaller, show the same trend and the same order of magnitude of those calculated on the new *ab initio* curve.

The V-E2 rate corresponding to case 1 (starting and ending on the same $^3\Pi$ PES) is higher than for the other cases, particularly at low temperature. However, rate coefficients for all V-E2 processes are sensibly smaller than those for V-E1 energy transfer. Crossings involving the $^1\Sigma, v = 1$ state (for instance, case 4: $(^3\Pi, v = 1) \rightarrow (^1\Sigma, v = 1) \rightarrow (^3\Pi, v = 0)$)

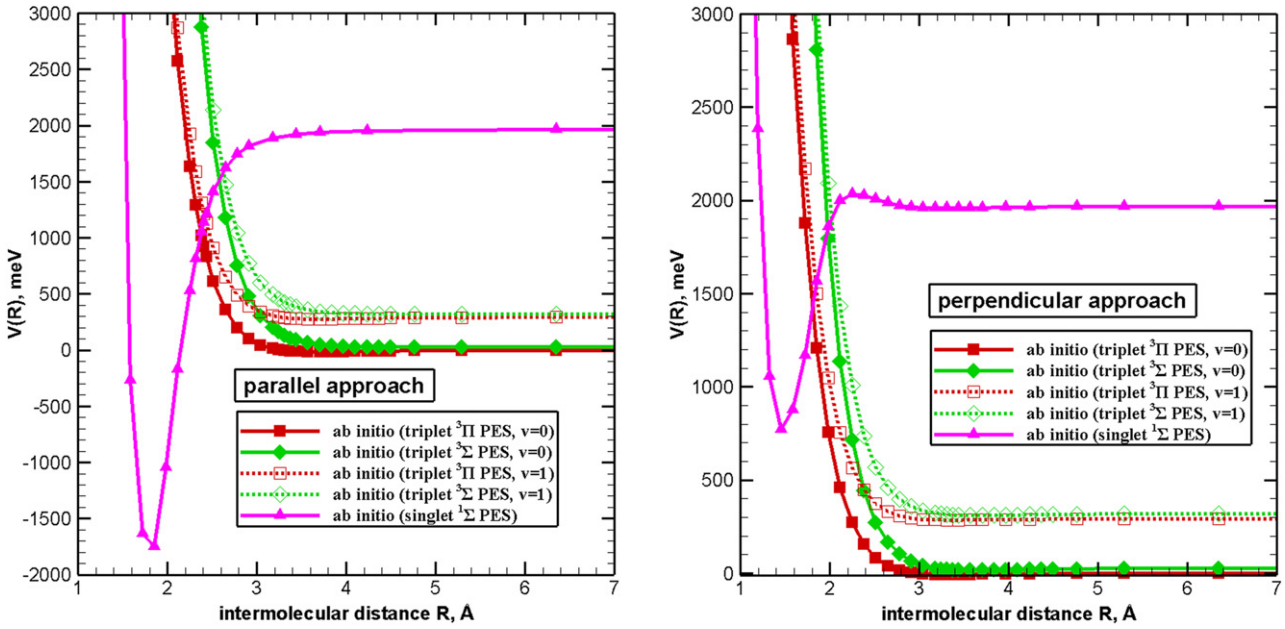

Figure 5. Behavior of *ab initio* potential energies as a function of the intermolecular distance R for the parallel (left) and perpendicular (right) configurations.

occur at higher energy and the corresponding rate coefficients are therefore lower (figure S3 in supporting information).

Figure 4 summarizes the rate coefficients for all the events (V-E1, V-E2 and previously calculated V–T rates [15]) determining the overall vibrational quenching of $N_2(v = 1)$ by $O(^3P)$ collisions, reported together with the available measured data (whose details are given in the figure caption) and the corresponding uncertainties, and allows to establish which processes are more effective in different temperature regimes. At $T \leqslant 3000$ K V-E1 process is predominant: the total rate coefficients for temperature lower than 2000 K are essentially those obtained for collisions occurring collinearly and they match very well with experimental data. As temperature increases, the contribution from the perpendicular configuration collisions becomes comparable, leading to calculated rate coefficients at $T \approx 3000$ K slightly larger than the experimental ones (still within their estimated uncertainty). At 4000 K V-E1 (which have now reached a plateau) and V–T processes become comparable and the sum of calculated rate coefficients for the processes gives an excellent match with measured vibrational quenching rates. Note that V-E2 rate coefficients are orders of magnitude smaller and their contribution to the overall vibrational relaxation process is negligible, conversely to what suggested in the literature. It is also interesting to remark that the discrepancy we found in reference [15] between calculated and experimental rate coefficients at $T \approx 4000$ K seems to be totally ascribable to the neglecting of the contribution coming from non collinear collisions. In the higher temperature regime ($T \geqslant 6000$ K) vibrational relaxation is completely determined by V–T events. A quantitative comparison between the calculated and experimental rate coefficients is given in table S6 and figure S4 in SI.

3.3. Vibrational relaxation for $N_2(v) + O \rightarrow N_2(v - 1) + O$

Rate coefficients for V–T processes involving the loss of one vibrational quantum, calculated on the $^3\Pi$ and $^3\Sigma$ PESs for v up to 10, as a function of temperature are shown in figure S5 and tables S4 and S5 in SI, whereas figure 6 shows the weight averaged (2:1 for $^3\Pi$ and $^3\Sigma$) ones. In all cases V–T rate coefficients strongly increase with temperature for temperature lower than 5000 K. Above this value, the increase gets milder and nearly reaches a plateau at the highest temperature investigated here. Rate coefficients also increase with the v quantum number, due to the decrease of the vibrational energy quantum. Differences can reach orders of magnitude at the lowest temperature, but they level up to few units factors at most, as the temperature increases. The trend and order of magnitude of the rate coefficients calculated on the $^3\Pi$ and $^3\Sigma$ PESs is similar, with those computed on the latter correspondingly lower.

We calculated V-E1 transitions for $(^3\Pi,\ v) \rightarrow (^3\Sigma,\ v' = v - 1)$ processes for v up to 10 using the same method described in the preceding section. The intermolecular distance, the energy and the absolute difference in the slope of the curves at the crossing points in the parallel and perpendicular configurations are shown in table 1 and are graphically displayed in figures 7 and S6 in the supporting information. As the vibrational quantum number v grows the intermolecular distance at which the crossing takes place becomes slightly longer and the potential energy at the crossing increases.

V-E1 transitions can be calculated by the original Landau–Zener method. Specifically, the total V-E1 probability for the $(^3\Pi,\ v = 2) \rightarrow (^3\Sigma,\ v = 1)$ transition is given as follows:

$$P_{(^3\Pi, v=2)\rightarrow(^3\Sigma, v=1)} = P_{2,1} \cdot \left(1 - P_{2,1}\right) + \left(P_{2,0}^2 + \left(1 - P_{2,0}\right)^2\right) \cdot P_{2,1} \cdot \left(1 - P_{2,1}\right), \quad (7)$$

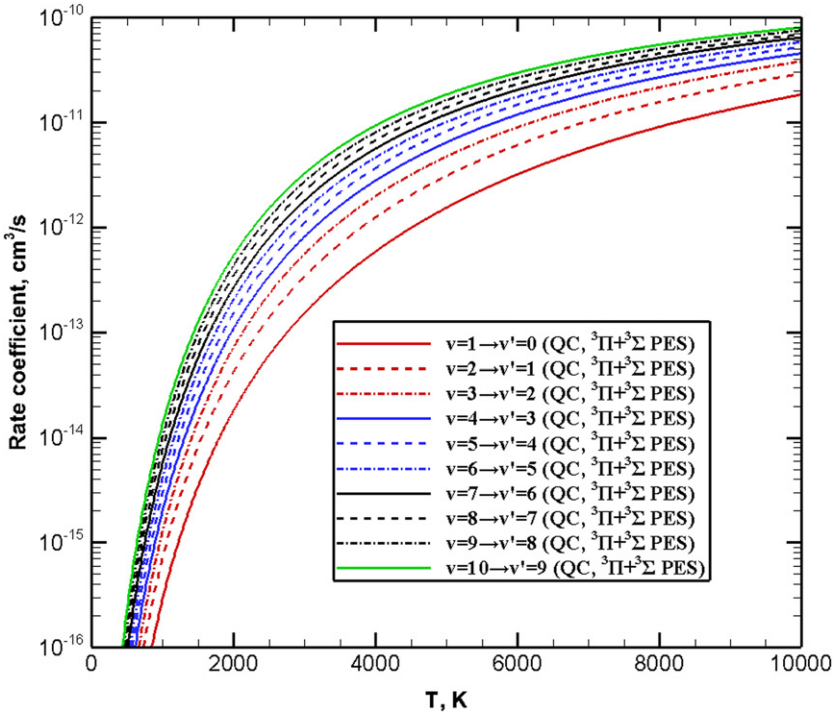

Figure 6. The averaged (2:1 for $^3\Pi$ and $^3\Sigma$) V–T rate coefficients for vibrational relaxation upon $N_2(X^1\Sigma_g^+) + O(^3P)$ collision as a function of temperature.

where P_i is the probability of staying on the same surface at the crossing point. Note that the calculation of the total probability of the $(^3\Pi, v = 2) \rightarrow (^3\Sigma, v = 1)$ process implies the knowledge of the probability of crossings between surfaces involving the loss of two vibrational quanta $P_{2,0}$ (with $\Delta v = 2$). However, as Δv grows, the crossing points occur at shorter R_c values, in a region where the present analytical $^3\Pi$ PES is less accurate, as shown in figure 1 (see the following section for a detailed description), and the related crossing probabilities (table 3) are expected to be correspondingly less accurate than those in table 1. Nevertheless, the formulation of equation (7) clearly shows that, because the $\Delta v = 2$ crossing is located much higher in energy than that $\Delta v = 1$ with the $(1 - P_{2,0})$ transition probability thus being much smaller than $(1 - P_{2,1})$, its accuracy has a minor effect on the whole $P_{(^3\Pi,v=2)\rightarrow(^3\Sigma,v=1)}$ determination.

The total V-E1 probability of $(^3\Pi, v = 3) \rightarrow (^3\Sigma, v = 2)$ is determined by

$$\begin{aligned} P_{(^3\Pi,v=3)\rightarrow(^3\Sigma,v=2)} &= P_{3,2}\cdot\left(1-P_{3,2}\right)+\left(1-P_{3,1}\right)^2\cdot P_{3,2} \\ &\cdot\left(1-P_{3,2}\right)+P_{3,1}^2\cdot P_{3,2}\cdot\left(1-P_{3,2}\right) \\ &\cdot\left(P_{3,0}^2+\left(1-P_{3,0}\right)^2\right), \end{aligned} \tag{8}$$

where terms involving vibronic crossings with $\Delta v = 2$, $P_{3,1}$, and $\Delta v = 3$, $P_{3,0}$, also come into play. The terms in the total probability involving the crossing with $\Delta v = 1$ are larger than the others and determine the main contribution in the sum.

The total V-E1 probability of $(^3\Pi, v = 4) \rightarrow (^3\Sigma, v = 3)$ is given by

$$\begin{aligned} &P_{(^3\Pi,v=4)\rightarrow(^3\Sigma,v=3)} \\ &\quad= P_{4,3}\cdot\left(1-P_{4,3}\right)+\left(1-P_{4,2}\right)^2\cdot P_{4,3}\cdot\left(1-P_{4,3}\right) \\ &\qquad+P_{4,2}^2\cdot P_{4,3}\cdot\left(1-P_{4,3}\right)\cdot\left(1-P_{4,1}\right)^2 \\ &\qquad+P_{4,2}^2\cdot P_{4,1}^2\cdot P_{4,3}\cdot\left(1-P_{4,3}\right)\cdot\left(P_{4,0}^2+\left(1-P_{4,0}\right)^2\right). \end{aligned} \tag{9}$$

The probability $1 - P_{4,0}$ (for crossing between $(^3\Pi, v = 4)$ and $(^3\Sigma, v = 0)$, not shown in the tables), as is the case for all processes with $\Delta v \geqslant 4$, is nearly zero, so that the corresponding term in the above sum can be neglected and the total V-E1 probability of $(^3\Pi, v = 4) \rightarrow (^3\Sigma, v = 3)$ can be simplified to

$$\begin{aligned} P_{(^3\Pi,v=4)\rightarrow(^3\Sigma,v=3)} &= P_{4,3}\cdot\left(1-P_{4,3}\right)+\left(1-P_{4,2}\right)^2\cdot P_{4,3} \\ &\cdot\left(1-P_{4,3}\right)+P_{4,2}^2\cdot P_{4,3}\cdot\left(1-P_{4,3}\right) \\ &\cdot\left(P_{4,1}^2+\left(1-P_{4,1}\right)^2\right). \end{aligned} \tag{10}$$

The V-E1 probabilities for $(^3\Pi, v) \rightarrow (^3\Sigma, v' = v - 1)$ processes with $v = 5, \ldots, 10$ can be obtained in a similar fashion, by neglecting terms involving the probability of crossings with $\Delta v \geqslant 4$. The crossing points between the involved vibronic PESs in parallel and perpendicular configurations are shown in

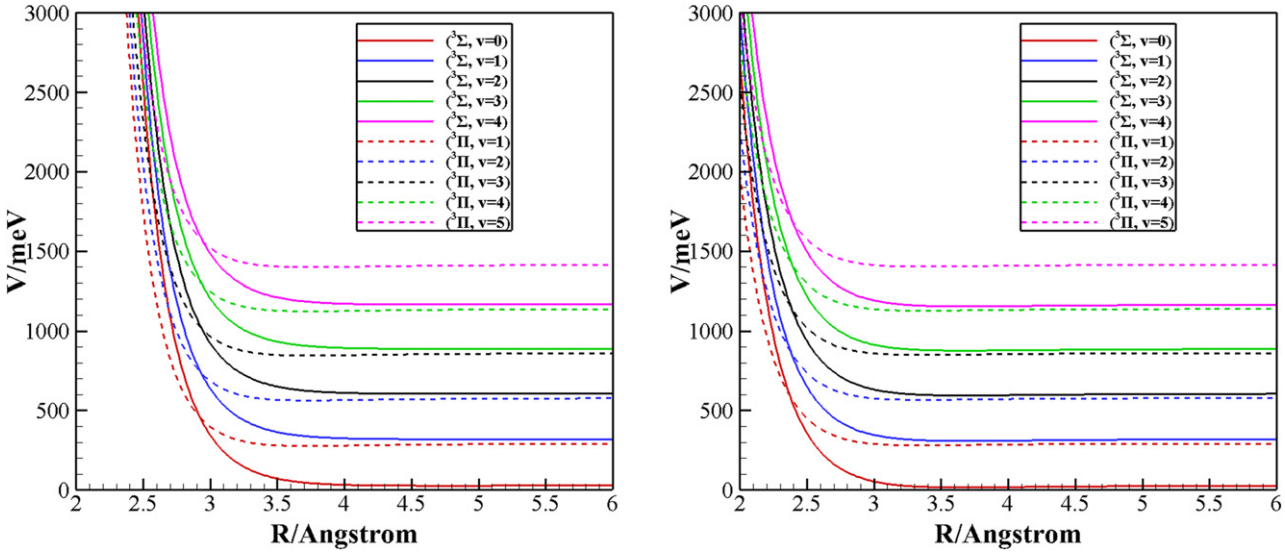

Figure 7. Potential energy curves for the $N_2(X^1\Sigma_g^+) + O(^3P)$ interaction with N_2 molecular axis oriented parallel (left panel) and perpendicular (right panel) to the intermolecular distance. The vibrational energy ($v = 1$ to 5 for the $^3\Pi$ state) is added to the potential curves.

figures 7 and S6 in the supporting information, and the details can be found in tables 1 and 3.

The V-E1 rate coefficients for $v = 2$ and $v = 3$ are shown in figure 8 and those for $v = 4, \ldots, 10$ in figure S7 in SI as a function of temperature. They all show a very similar behavior to V-E1 rate coefficients for $v = 1$, with the contribution of the perpendicular configuration being much smaller than the parallel one at low temperature and becoming comparable at $T \geqslant 4000$ K ca. A strong increase with temperature is observed at the lowest T to reach a plateau at 2000 K ca.

V-E2 non-adiabatic energy transfer from the $^3\Pi$ (or the $^3\Sigma$) to the $^1\Sigma$ state when $\Delta v = 1$ is expected to be comparable to that for the $v = 1$ case, which was found to be negligible with respect to V–T and V-E1. Therefore V-E2 rates were not evaluated.

Figures 8 and S7 in SI also report total vibrational relaxation rate coefficients, showing the same behavior of figure 4 for $v = 1$: V–T and V–E events emerge in different ranges of gas mixture temperatures. At low temperature V-E1 energy transfer dominates and at high temperature vibrational quenching is only due to V–T processes. The temperature at which the two regimes switch, i.e. where the V–T and V-E1 contributions are comparable, lowers as v increases: V–T prevails at $T \geqslant 4000$ K ca. for $v = 1$ and at $T \geqslant 2000$ K ca. for $v = 10$. The reason for such behavior is mainly connected to the V–T rate coefficients which increase with the v quantum number, whereas V-E1 ones are substantially independent on v (only a very slight increase can be observed).

Rate coefficients for vibrational relaxation are needed for the kinetic modelling of gas mixture flows at different temperature conditions. We therefore fitted the total rate coefficients of $N_2(X^1\Sigma_g^+, v) + O(^3P) \rightarrow N_2(X^1\Sigma_g^+, v-1) + O(^3P)$ vibrational relaxation for $v = 1$–10 to a general analytical expression for rate coefficients as a function of temperature as:

$$k_{v\rightarrow v-1}(T) = \exp\left(\frac{a_{-1}}{T} + a_0 + a_1 T + a_2 T^2 + a_3 T^3 + a_4 T^4\right). \quad (11)$$

The form of the above formulation is obtained from the symbolic regression [48] by searching the space of mathematical expressions while minimizing the absolute error metric. Since the vibrational relaxation rate in the whole temperature range explored here is in fact the result of two different processes, a general Arrhenius form cannot fit the total rate coefficients. The fitting coefficients in equation (11), obtained by a least square procedure, are listed in table 4, and the valid range of temperature is 200–10000 K. Figure S8 in SI reports the comparison between calculated rate coefficients for $v = 1$, 5 and 10 and those obtained by the analytical expression of equation (11) and shows that the latter is able to capture the transition between the two different temperature dependencies of the overall vibrational quenching.

3.4. Vibrational relaxation for $N_2(v) + O \rightarrow N_2(v - \Delta v) + O$

V–T rate coefficients for collisions involving the loss of two vibrational energy quanta (figure 8, for initial $v = 2$ and $v = 3$) are smaller than those obtained for $\Delta v = 1$ of about one order of magnitude at the highest temperature investigated here and up to several orders of magnitude as the temperature decreases. The probability for processes where $\Delta v = 3$ becomes correspondingly lower (figure S6 in SI). Tables with V–T rate coefficients at selected temperature values for $\Delta v = 1, 2, 3$ calculated on the $^3\Pi$ (table S4) and on the $^3\Sigma$ PES (table S5) are reported in the supporting information.

V-E1 crossings between the $^3\Pi$ and $^3\Sigma$ surfaces involving the loss of two vibrational quanta occur at higher energies, making these events less probable at the temperature considered in the present study, and at shorter intermolecular distances than those with $\Delta v = 1$. This might lead to accuracy

Table 3. Crossing points in parallel and perpendicular configurations for non adiabatic transitions with $\Delta v = 2$ and $\Delta v = 3$: R_c is the position, E_c is the potential energy and Δ is the absolute difference of the curve slopes.

		Parallel			Perpendicular		
Crossing point between	P_x	R_c (Å)	E_c (eV)	Δ (eV Å^{-1})	R_c (Å)	E_c (eV)	Δ (eV Å^{-1})
$\left({}^3\prod, v=2\right)$ and $\left({}^3\sum, v=0\right)$	$P_{2,0}$	2.688	1.146	1.855	2.162	1.382	1.947
$\left({}^3\prod, v=3\right)$ and $\left({}^3\sum, v=1\right)$	$P_{3,1}$	2.698	1.411	1.766	2.167	1.645	1.947
$\left({}^3\prod, v=3\right)$ and $\left({}^3\sum, v=0\right)$	$P_{3,0}$	2.567	1.902	2.927	2.047	2.225	3.042
$\left({}^3\prod, v=4\right)$ and $\left({}^3\sum, v=2\right)$	$P_{4,2}$	2.698	1.679	1.766	2.172	1.908	1.856
$\left({}^3\prod, v=4\right)$ and $\left({}^3\sum, v=1\right)$	$P_{4,1}$	2.572	2.157	2.927	2.052	1.334	3.042
$\left({}^3\prod, v=5\right)$ and $\left({}^3\sum, v=3\right)$	$P_{5,3}$	2.703	1.942	1.682	2.176	2.169	1.856
$\left({}^3\prod, v=5\right)$ and $\left({}^3\sum, v=2\right)$	$P_{5,2}$	2.576	2.411	2.779	2.056	2.725	2.892
$\left({}^3\prod, v=6\right)$ and $\left({}^3\sum, v=4\right)$	$P_{6,4}$	2.707	2.202	1.682	2.180	2.427	1.856
$\left({}^3\prod, v=6\right)$ and $\left({}^3\sum, v=3\right)$	$P_{6,3}$	2.580	2.663	2.779	2.059	2.974	2.892
$\left({}^3\prod, v=7\right)$ and $\left({}^3\sum, v=5\right)$	$P_{7,5}$	2.711	2.459	1.682	2.183	2.682	1.768
$\left({}^3\prod, v=7\right)$ and $\left({}^3\sum, v=4\right)$	$P_{7,4}$	2.583	2.911	2.779	2.063	3.220	2.892
$\left({}^3\prod, v=8\right)$ and $\left({}^3\sum, v=6\right)$	$P_{8,6}$	2.716	2.712	1.603	2.187	2.932	1.768
$\left({}^3\prod, v=8\right)$ and $\left({}^3\sum, v=5\right)$	$P_{8,5}$	2.588	3.157	2.638	2.067	3.462	2.750
$\left({}^3\prod, v=9\right)$ and $\left({}^3\sum, v=7\right)$	$P_{9,7}$	2.720	2.962	1.603	2.191	3.180	1.768
$\left({}^3\prod, v=9\right)$ and $\left({}^3\sum, v=6\right)$	$P_{9,6}$	2.592	3.399	2.638	2.071	3.701	2.750
$\left({}^3\prod, v=10\right)$ and $\left({}^3\sum, v=8\right)$	$P_{10,8}$	2.724	3.208	1.603	2.195	3.424	1.685
$\left({}^3\prod, v=10\right)$ and $\left({}^3\sum, v=7\right)$	$P_{10,7}$	2.596	3.638	2.638	2.074	3.937	2.750

issues when the present $^3\Pi$ surface is used. The ILJ model in fact gives a good description of the potential for medium and long range interaction regions, including wells and first repulsive walls, whereas the short range strong interaction region might not be as accurately represented, particularly when chemical forces are operative, opening reactive channels. Figure 2 shows that the match between the non reactive $^3\Sigma$ PES and the corresponding *ab initio* points, though slightly decreasing, remains good at intermolecular distance R values as short as 2 Å. The $^3\Pi$ surface, on the other hand, where the reactive channel N(^{4}S) + NO($^2\Pi$) opens at lower energies, presents a more relevant discrepancy with *ab initio* points at $R \leqslant 2.5$ Å. As a consequence, a larger uncertainty is associated to the determination of distance, energy and slope (even if the slopes of the analytical $^3\Pi$ PES and the *ab initio* points remain similar) of the crossing points reported in table 3.In addition,as Δv increases, Franck–Condon factors can be appreciably smaller than unity, so that the V-E1 rate coefficients reported here are intended to be semi-quantitative, i.e. they are expected to have the correct order of magnitude, but their absolute value is only indicative.

The total probability of ($^3\Pi$, v) $\rightarrow$ ($^3\Sigma$, $v - \Delta v$) can be obtained according to the Landau–Zener approach, similarly to equations (7) and (10), and the relative V-E1 rate coefficients for $v = 2$ and $v = 3$ can be found in figure 8, together with V–T and total relaxation rates. V-E1 rate coefficients for transitions with $\Delta v = 2$ show the same trend as those with $\Delta v = 1$, but they reach a plateau at higher temperature and are consistently smaller (less than one order of magnitude at the plateau to up to several orders of magnitude at the lowest temperature). The overall vibrational quenching is again dominated by V-E1 processes at low and by V–T ones at high temperature values. The switch from one regime to the other shifts to higher temperature as Δv grows.

Table 4. Fitting coefficients to the analytic expression (equation (11)) of the total vibrational quenching rate coefficient $k_{v\to v-1}(T)$ for the loss of a vibrational energy quantum as a function of temperature.

v	a_{-1}	a_0	a_1	a_2	a_3	a_4
1	-1.97×10^{3}	-27.9	-5.07×10^{-5}	1.09×10^{-7}	-8.46×10^{-12}	1.48×10^{-16}
2	-2.00×10^{3}	-28.0	0.00	1.58×10^{-7}	-1.78×10^{-11}	5.92×10^{-16}
3	-1.78×10^{3}	-28.0	-1.01×10^{-4}	2.44×10^{-7}	-3.18×10^{-11}	1.26×10^{-15}
4	-1.73×10^{3}	-28.1	0.00	2.48×10^{-7}	-3.49×10^{-11}	1.46×10^{-15}
5	-1.68×10^{3}	-28.1	0.00	2.86×10^{-7}	-4.25×10^{-11}	1.86×10^{-15}
6	-1.63×10^{3}	-28.1	1.04×10^{-4}	2.71×10^{-7}	-4.22×10^{-11}	1.89×10^{-15}
7	-1.58×10^{3}	-28.4	4.11×10^{-4}	1.95×10^{-7}	-3.45×10^{-11}	1.60×10^{-15}
8	-1.53×10^{3}	-28.6	8.90×10^{-4}	8.36×10^{-9}	-8.16×10^{-12}	3.79×10^{-16}
9	-1.53×10^{3}	-28.5	6.51×10^{-4}	1.47×10^{-7}	-3.13×10^{-11}	1.55×10^{-15}
10	-1.47×10^{3}	-28.7	9.24×10^{-4}	7.68×10^{-8}	-2.39×10^{-11}	1.27×10^{-15}

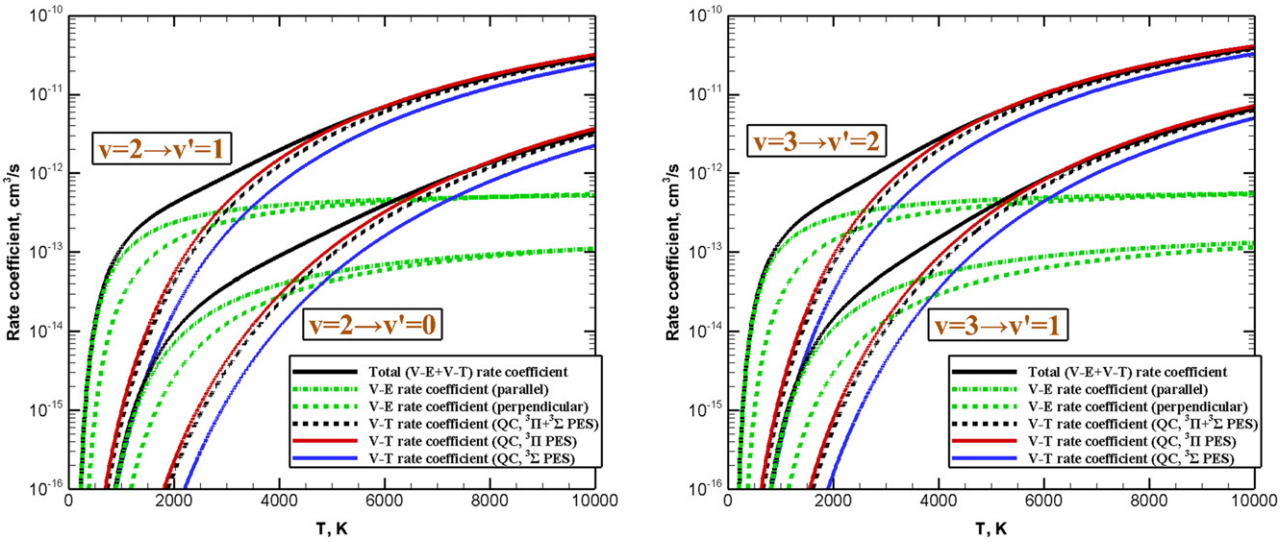

Figure 8. V–T, V-E1 and total relaxation rate coefficients for the $N_2(X^1\Sigma_g^+, v) + O(^3P) \to N_2(X^1\Sigma_g^+, v') + O(^3P)$ collision for $v = 2$ (left panel) and $v = 3$ (right panel) as a function of temperature.

4. Conclusions and perspectives

Recent evidence indicates that the solution of the apparent discrepancy between theoretical and measured rate coefficients for the $N_2(v = 1) + O(^3P) \to N_2(v = 0) + O(^3P)$ inelastic collisions comes from the inclusion of V–E transfer processes between low-lying PESs of different spin–orbit and electronic states. This prompted us to extend the developed methodology to include higher excited vibrational states of molecular nitrogen and to evaluate the contribution of the non-adiabatic crossing between triplet and singlet surfaces.

Rate coefficients for the vibrational relaxation of $N_2(v)$ colliding with $O(^3P)$ atoms were thus calculated considering v values up to 10. In details, V–T rates were computed by using a MQC method, whereas V–E rates were evaluated through Landau–Zener approaches. Results show that in all cases vibrational relaxation at low temperature is mainly determined by the V–E energy transfer occurring at the crossing between the $^3\Pi$ and $^3\Sigma$ PESs, and V–T energy transfer becomes predominant as the temperature increases. Non-adiabatic energy transfer between the vibronic $^3\Pi/^3\Sigma$ and the excited $^1\Sigma$ PES was also considered and demonstrated that its involvement in vibrational quenching for the processes considered here (with $\Delta v = 1, 2$) is negligible.

Calculated rate coefficients for the $N_2(v = 1) + O(^3P) \to N_2(v = 0) + O(^3P)$ vibrational relaxation give an excellent agreement with available experimental data in the whole temperature range, highlighting the need of a detailed description of both V–T and V–E processes. We expect that the rates corresponding to the $N_2(v) + O(^3P) \to N_2(v - 1) + O(^3P)$ process, involving the loss of one vibrational quantum, should be as accurate as those for $v = 1$, because, as v grows, the crossing points between $^3\Pi$ and $^3\Sigma$ PESs occur at larger $N_2(v = 1) + O(^3P)$ interaction distances, where the analytical PESs

provide a better description. Calculated V-E1 rate coefficients for multiquantum relaxation processes are instead only meant to give the correct order of magnitude, because of the larger uncertainty related to their determination.

Indeed, as discussed in the above sections, the uncertainty associated to the evaluation of the rates of the various processes contributing to overall quenching can be quite different. In particular, two main issues can be identified as possible sources of uncertainty. On one side, as Δv increases the crossings between the $^3\Pi$ and $^3\Sigma$ PESs occur at shorter interaction distances and at higher potential energy value. In the short range strong interaction region the non-reactive representation of the employed PESs (particularly the $^3\Pi$ one) is bound to be less appropriate, since covalent forces emerge with the opening of reactive channels. It is worth noting that such uncertainty has much less effect on the determination of V–T rates, which are instead more sensitive to the long range potential. In addition, as shown in figure 2, though the absolute difference with *ab initio* calculated energies can be relevant, the PESs slope, driving the V–T dynamics, is still close to the *ab initio* points.

To correctly describe both V–T and V–E processes, it would be desirable to have PESs able to accurately represent the short range region, with the opening of reactive channels, as well as the long range region, determinant for the formation of weakly interacting precursor species. However, *ab initio* based potentials, describing in details covalent interactions, can seldom cover the longest interaction regions, and analytical formulations, giving a reliable description of weak interactions, cannot be used to model chemical forces. The possibility of using a smoothly combined PES [49], which could merge the benefits of both representations, is currently under investigation. Such PES, together with QCT or a MQC code properly including reactivity [50], would allow to consider the competition between reactive channels and vibrational quenching and the contribution of quasi reactive events to vibrational relaxation [20], therefore permitting to calculate reliable relaxation rates for very high v values (up to $v \approx 40$).

The other uncertainty source comes from the use of Landau–Zener model to calculate V–E probabilities and cross sections. The determination of the involved parameters can be a difficult task, as Δv grows. The coupling term H depends on the position and orientation of the interacting species at the crossing points and must include the associated Franck–Condon factors, that sensibly decrease with the increase in Δv. Besides, we showed here that, though the collinear orientation gives the main contribution to V–E processes at very low temperature, contributions coming from other geometries cannot be neglected as temperature rises. Therefore, a more sophisticated dynamical model (such as trajectory surface hopping) should be used to have a more accurate determination of V–E rate coefficients in such conditions.

Acknowledgments

This work was supported by the Strategic Priority Research Program of Chinese Academy of Sciences (Grant No. XDA17030100) and the National Natural Science Foundation of China through Grants 11372325 and 91116013. MB acknowledges the PID2020-114654GB-I00 Spanish grant for funding.

Data availability statement

All data that support the findings of this study are included within the article (and any supplementary files).

Appendix A. Landau–Zener determination of *P*(*x*) probabilities

A.1. Details and parameters for V-E1 Landau–Zener method

In the range of collision energies associated to the temperature of interest here (below 10 000 K), the use of a fixed value of H is sufficient to calculate reliable cross sections and rate coefficients. The exact determination of the value of H is a complicated task. However, physical considerations allow to foresee that H should be comprised between 1–2 meV, a very small value, which in practice prevents its computation by *ab initio* methods, as it falls within the accuracy of the highest available levels of theory. The coupling is expected to be small, because it occurs between two heterogeneous (i.e. corresponding to different Σ and Π symmetries) surfaces, which also ensures the validity of the Landau–Zener approach. Furthermore, H is the result of two contributions: the spin–orbit coupling, estimated to be slightly larger than in the O + Ar case [26] where the electrostatic contribution is absent, for which the first order non-adiabatic correction to adiabatic potential is around 0.2 meV, and the Coriolis coupling, which should be ≈1 meV, the value corresponding to a collision with an impact parameter of 1 Å at a relative velocity of 1.5 km s^{-1} [51]. Given the empirical nature of such an estimate, the same value of $H = 1.5$ meV used in [15] was considered for both parallel and perpendicular contribution to V–E, even if the exact H value depends on the intermolecular distance R and on the reciprocal orientation of the colliding partners. This value has been used for all the V-E1 rate coefficients calculations. Because of these approximations V–E rate coefficients obtained here are expected to be less accurate (with an estimated accuracy of about 40%–50%) than V–T rates for the homologous processes.

The radial velocity v_R at the crossing in equation (4) is given by:

$$v_R^2 = \frac{2}{\mu}\left(E - \frac{\hbar^2(l+1)l}{2\mu R_c^2} - E_x\right), \tag{12}$$

where l is the quantum number representing the orbital angular momentum of the collision complex (from 0 to l_{max}, which guarantees v_R to be real), μ is the reduced mass and E is the collision energy. E_x is the potential energy in the entrance channel, i.e. the difference between the energy at the crossing point, E_c, and the vibrational energy E_v of N_2 (for $v = 1$, $E_v = 0.2926$ eV).

A.2. Details and parameters for V-E2 modified Landau–Zener method

A special treatment is needed when the curves cross with opposite sign slopes. Equation (5) gives the transition probability in the modified Landau–Zener method, depending on the following parameters:

$$\varepsilon = E_s(F_1 - F_2)/2FH, \tag{13}$$

$$\beta = \frac{4H}{\hbar}\left[\frac{\mu H}{F(F_1 - F_2)}\right]^{1/2}, \tag{14}$$

$$E_s = E - \frac{\hbar^2(l+1)l}{2\mu R_c^2} - E_x, \quad F = \left(|\Psi_1 \cdot \Psi_2|\right)^{1/2}, \tag{15}$$

$$\Psi_i = F_i - \frac{\hbar^2(l+1)l}{2\mu R_c^2}\frac{2}{R_c}, \tag{16}$$

where F_i is the slope of the curve, l is the orbital angular momentum quantum number, μ is reduced mass and E is collision energy. Moreover, E_x represents the difference between the energy at the crossing point, E_c, and the vibrational energy E_v of N_2, R_c is the intermolecular distance at the crossing point and H is the non-adiabatic coupling. Note that a factor $\frac{1}{\hbar}$ is missing in the corresponding expression in reference [47].

The value of non adiabatic spin–orbit coupling H between the singlet and the triplet PESs along the crossing seam adopted here was taken from reference [34]: $H = 85$ cm^{-1} and 65 cm^{-1} for the parallel and perpendicular configurations, respectively. In these estimates the Coriolis coupling is not considered. The proposed H value for the parallel configuration is consistent with the electronic transition matrix element proposed by Fisher and Bauer [27]

$$V_{12}^{el}(R_c) \approx V_{12}^{el}(R \to \infty) = V^{el}\left\{O\left(^1D_2 - {}^3P_2\right)\right\} = 80 \text{ cm}^{-1}, \tag{17}$$

in which the electronic transition matrix element is considered to be the spin–orbit coupling value of the isolated oxygen atom and equal to 80 cm^{-1} [52].

ORCID iDs

Qizhen Hong https://orcid.org/0000-0003-3188-9167
Massimiliano Bartolomei https://orcid.org/0000-0001-8643-4106
Fernando Pirani https://orcid.org/0000-0003-3110-6521
Fabrizio Esposito https://orcid.org/0000-0003-0586-5866
Quanhua Sun https://orcid.org/0000-0002-0008-1790
Cecilia Coletti https://orcid.org/0000-0002-3609-290X

References

[1] Adamovich I *et al* 2017 *J. Phys. D: Appl. Phys.* **50** 323001
[2] Guerra V, Tejero-del-Caz A, Pintassilgo C D and Alves L L 2019 *Plasma Sources Sci. Technol.* **28** 073001
[3] Capitelli M, Celiberto R, Colonna G, Esposito F, Gorse C, Hassouni K, Laricchiuta A and Longo S 2016 *Kinetic and Monte Carlo Approaches to Solve Boltzmann Equation for the Electron Energy Distribution Functions* (Berlin: Springer) pp 79–111
[4] Capitelli M *et al* 2012 *Plasma Chem. Plasma Process.* **32** 427–50
[5] Colonna G, Laporta V, Celiberto R, Capitelli M and Tennyson J 2015 *Plasma Sources Sci. Technol.* **24** 035004
[6] Adamovich I V and Lempert W R 2015 *Plasma Phys. Control. Fusion* **57** 014001
[7] Schwartzentruber T E and Boyd I D 2015 *Prog. Aerosp. Sci.* **72** 66–79 Celebrating 60 Years of the Air Force Office of Scientific Research (AFOSR): A Review of Hypersonic Aerothermodynamics
[8] Celiberto R *et al* 2016 *Plasma Sources Sci. Technol.* **25** 033004
[9] Keidar M 2015 *Plasma Sources Sci. Technol.* **24** 033001
[10] Rouwenhorst K H R, Jardali F, Bogaerts A and Lefferts L 2021 *Energy Environ. Sci.* **14** 2520–34
[11] Yankovsky V and Vorobeva E 2020 *Atmosphere* **11** 116
[12] Hong Q, Sun Q, Bartolomei M, Pirani F and Coletti C 2020 *Phys. Chem. Chem. Phys.* **22** 9375–87
[13] Hong Q, Sun Q, Pirani F, Valentín-Rodríguez M A, Hernández-Lamoneda R, Coletti C and Hernández M I 2021 *J. Chem. Phys.* **154** 064304
[14] Hong Q, Bartolomei M, Coletti C, Lombardi A, Sun Q and Pirani F 2021 *Molecules* **26** 7152
[15] Hong Q, Bartolomei M, Esposito F, Coletti C, Sun Q and Pirani F 2021 *Phys. Chem. Chem. Phys.* **23** 15475–9
[16] Van Alphen S, Vermeiren V, Butterworth T, van den Bekerom D C M, van Rooij G J and Bogaerts A 2020 *J. Phys. Chem.* C **124** 1765–79
[17] Breshears W D and Bird P F 1968 *J. Chem. Phys.* **48** 4768–73
[18] Eckstrom D J 1973 *J. Chem. Phys.* **59** 2787–95
[19] McNeal R J, Whitson M E and Cook G R 1972 *Chem. Phys. Lett.* **16** 507–10
[20] Esposito F and Armenise I 2017 *J. Phys. Chem.* A **121** 6211–9
[21] Denis-Alpizar O, Bemish R J and Meuwly M 2017 *Phys. Chem. Chem. Phys.* **19** 2392–401
[22] Koner D, San Vicente Veliz J C, Bemish R J and Meuwly M 2020 *Phys. Chem. Chem. Phys.* **22** 18488–98
[23] Ivanov M V, Schinke R and Mcbane G C 2007 *Mol. Phys.* **105** 1183–91
[24] Schönherr T, Komurasaki K, Romano F, Massuti-Ballester B and Herdrich G 2015 *IEEE Trans. Plasma Sci.* **43** 287–94
[25] Nikitin E E and Umanski S Y 1972 *Faraday Discuss. Chem. Soc.* **53** 7–17
[26] Aquilanti V, Candori R and Pirani F 1988 *J. Chem. Phys.* **89** 6157–64
[27] Fisher E R and Bauer E 1972 *J. Chem. Phys.* **57** 1966–74
[28] Herzberg G 1945 *Molecular Spectra and Molecular Structure* (*Infrared and Raman Spectra of Polyatomic Molecules* vol 2) (Princeton, NJ: Van Nostrand-Reinhold)
[29] Gamallo P, González M and Sayós R 2003 *J. Chem. Phys.* **119** 2545–56
[30] Lin W, Varga Z, Song G, Paukku Y and Truhlar D G 2016 *J. Chem. Phys.* **144** 024309
[31] Luo H, Kulakhmetov M and Alexeenko A 2017 *J. Chem. Phys.* **146** 074303
[32] Koner D, Bemish R J and Meuwly M 2020 *J. Phys. Chem.* A **124** 6255–69
[33] Pirani F, Brizi S, Roncaratti L F, Casavecchia P, Cappelletti D and Vecchiocattivi F 2008 *Phys. Chem. Chem. Phys.* **10** 5489–503
[34] Nakamura H and Kato S 1999 *J. Chem. Phys.* **110** 9937–47
[35] González M, Valero R and Sayós R 2000 *J. Chem. Phys.* **113** 10983–98
[36] Li J and Varandas A J C 2012 *J. Phys. Chem.* A **116** 4646–56 PMID: 22494780
[37] Bartolomei M, Hernández M I, Campos-Martínez J, Carmona-Novillo E and Hernández-Lamoneda R 2008 *Phys. Chem. Chem. Phys.* **10** 5734

[38] Bartolomei M, Carmona-Novillo E, Campos-Martínez J, Hernández M I and Hernández-Lamoneda R 2010 *J. Chem. Phys.* **133** 12431
[39] Bartolomei M, Carmona-Novillo E, Hernández M I, Pérez-Ríos J, Campos-Martínez J and Hernández-Lamoneda R 2011 *Phys. Rev.* B **84** 092105
[40] Werner H-J *et al* 2012 MOLPRO, version 2012.1, a package of *ab initio* programs (see https://molpro.net)
[41] Billing G D 1984 *Comput. Phys. Commun.* **32** 45–62
[42] Landau L-D 1932 *Phys. Z. Sowjetunion* **2** 46–51
[43] Zener C 1932 *Proc. R. Soc. London* A **137** 696–702
[44] Stückelberg E C G 1932 *Helv. Phys. Acta* **5** 369–423
[45] Billing G D 1987 *Comput. Phys. Commun.* **44** 121–36
[46] Coveney P V, Child M S and Barany A 1985 *J. Phys. B: At. Mol. Phys.* **18** 4557
[47] Tosi P, Dmitrijev O, Soldo Y, Bassi D, Cappelletti D, Pirani F and Aquilanti V 1993 *J. Chem. Phys.* **99** 985–1003
[48] Koza J R 1994 *Stat. Comput.* **4** 87–112
[49] Martí C, Laganà A, Pacifici L, Pirani F and Coletti C 2021 *Chem. Phys. Lett.* **769** 138404
[50] Coletti C and Billing G D 2000 *J. Chem. Phys.* **113** 11101–8
[51] Aquilanti V, Candori R, Pirani F and Ottinger C 1994 *Chem. Phys.* **187** 171–83
[52] Yamanouchi T and Horie H 1952 *J. Phys. Soc. Japan* **7** 52–7